Electronic Supplementary Material (ESI) for Chemical Science.

Supporting Information

Photo-induced carbocation-enhanced charge transport in single-molecule junctions

Zhongwu Bei,[b] Yuan Huang,[b] Yangwei Chen,[b] Yiping Cao,*[b] Jin Li*[a]

[a] College of Chemistry, Research Center for Analytical Sciences, Nankai University, Tianjin 300071, China.
[b] Key Laboratory of Optoelectronic Chemical Materials and Devices of Ministry of Education, Jianghan University, Wuhan 430056, China.

Table of Contents

1. ^{1}H NMR Data

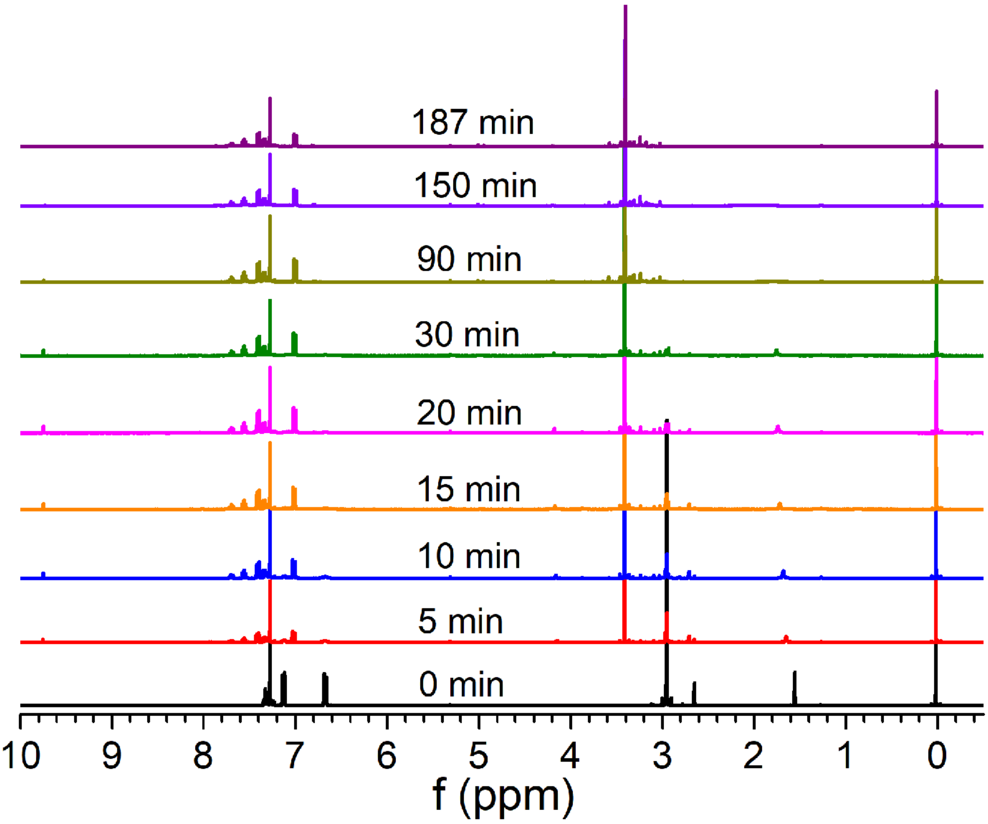

Figure S1. ^{1}H-NMR spectra ($CDCl_3$, 400M) of MGOH irradiated with 302-nm UV light with different time.

2. ESI-MS spectra of MGOH and MG⁺

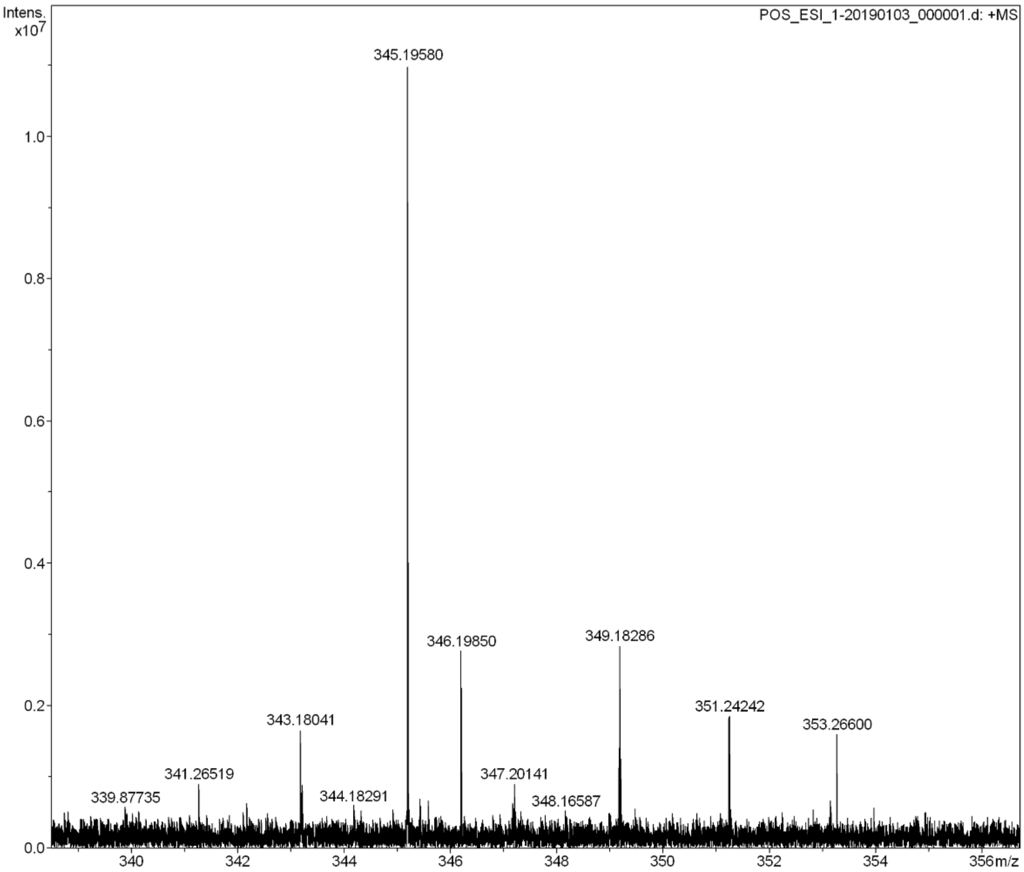

Figure S2. ESI-MS spectra of MGOH. Calculated M(MGOH)=346.20, ESI, found: m/z 345.19580: [M - H]$^-$; 346.19850: [M]$^+$.

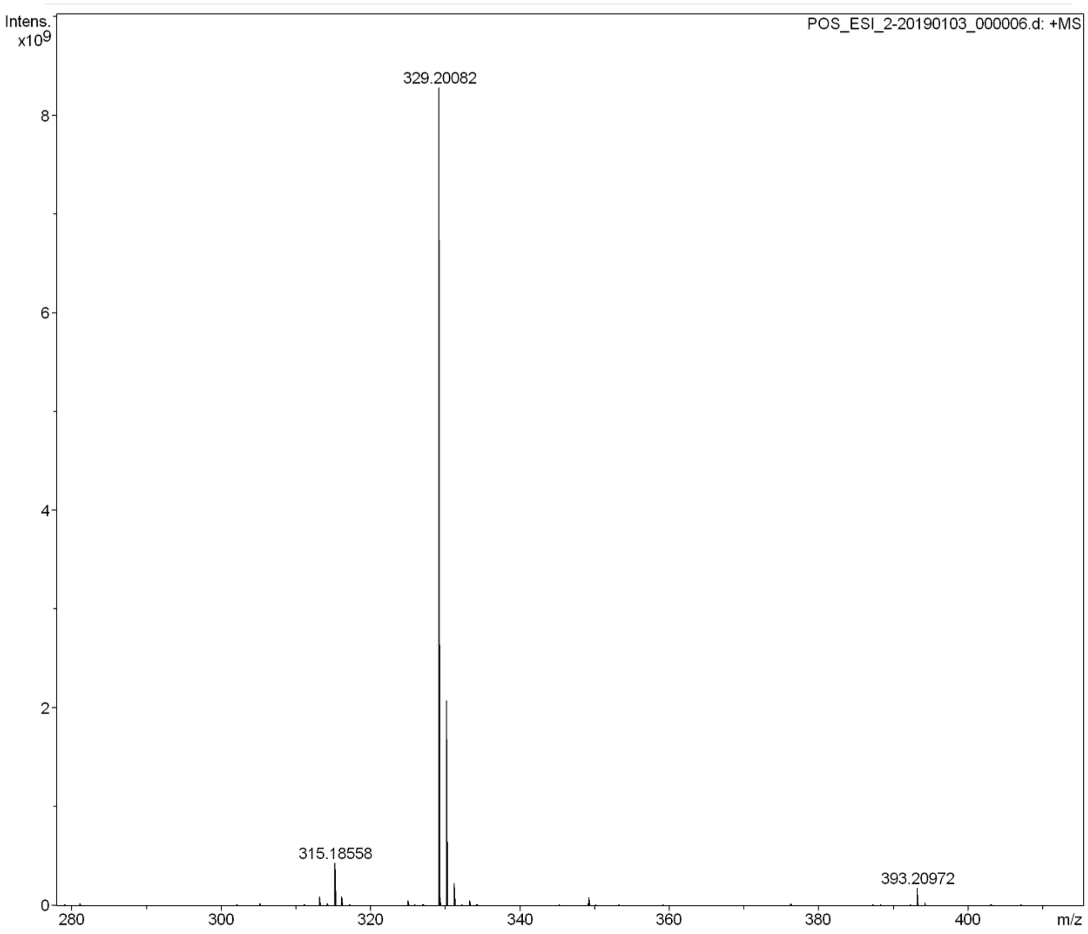

Figure S3. ESI-MS spectra of carbocations. Calculated M(MG^+) = 329.20, ESI, found: m/z 329.20082: $[M]^+$.

3. STM-BJ experiments

All reagents were commercially available and used without further purification: tetrahydrofuran (THF, ≥ 99.9%, Sigma-Aldrich), mesitylene (TMB, 98%, Sigma-Aldrich), MGOH (malachite green carbinol base, BS, Tianjin xi 'en si biochemical technology co., LTD). Electron spray ionization mass spectra (ESI-MS) were recorded on a JMS-LC mate mass spectrometer. Photo-radiated experiments were performed using a UVP Blak-Ray 12 W, 302 nm UV lamp (115 V, 60 Hz, 1400 $\mu m/cm^2$). In this case, the lamp was placed above the sample cell at a distance of 2 cm.

Before the experiment, the Au electrode was annealed in a hydrogen flame for 2 minutes, quenched in ultrapure water, followed by drying with an argon stream. A teflon liquid cell and teflon O-ring, pre-cleaned with Piranha solution, were assembled onto the Au electrode. The STM tips were mechanically cut Au wire (0.25 mm in diameter), leaving the very end of tip apex exposed to solution. The STM tips were covered with Apiezon wax in a high-polar solution such as aqueous solution, but not in a low-polar solution (such as THF/TMB, 1:4). The STM-BJ setup is shown in Figure S4. It is composed of motor (1), tip (2), Au electrode (3), the teflon liquid cell and teflon O-ring (4), Peltier heater (5), and so on. The temperature of the testing solutions was precisely controlled at 25 ^{o}C by using a Peltier heater to heat the substrate. Details of the STM-BJ measurement are described elsewhere.[1] A solution containing 0.1 mM of the target molecule in a mixture of THF and TMB, 1:4 (v/v) were added to the cell for break junction experiments. Most of the molecules investigated need the polar solvent to enhance their solubility, but the polar solvent, THF, will increase the leakage current and increase the noise floor. Therefore, introducing the non-polar solvent, TMB, is to lower the background noise of the conductance measurement. A constant bias potential (V bias) of 100 mV was applied between the tip and Au electrode. Then, the tip controlled by piezo actuator moved toward the Au electrode until connected with molecule or electrode, and then it got back (return). The stretching process was automatically repeated to generate a number of conductance versus distance traces. The presence of conductance steps in the conductance-distance traces corresponded to the formation of molecular junctions, in which the electrical conductance through the junction remains approximately constant as the electrode separation increases. During the break junction process, leakage currents[2] are also generated. The leakage current, which originates from the direct transmission of electrons under a low bias voltage from the source to drain terminal in vacuum or pure solvent conditions, is ubiquitous at the single-molecule level and exponentially increases with a reduction of the separation between the two electrodes. With the ability to accurately tune nanogap distance between the two-terminal devices, STM-BJ techniques facilitate the extraction of intrinsic molecular tunneling properties from tunneling leakage current for further data analysis.

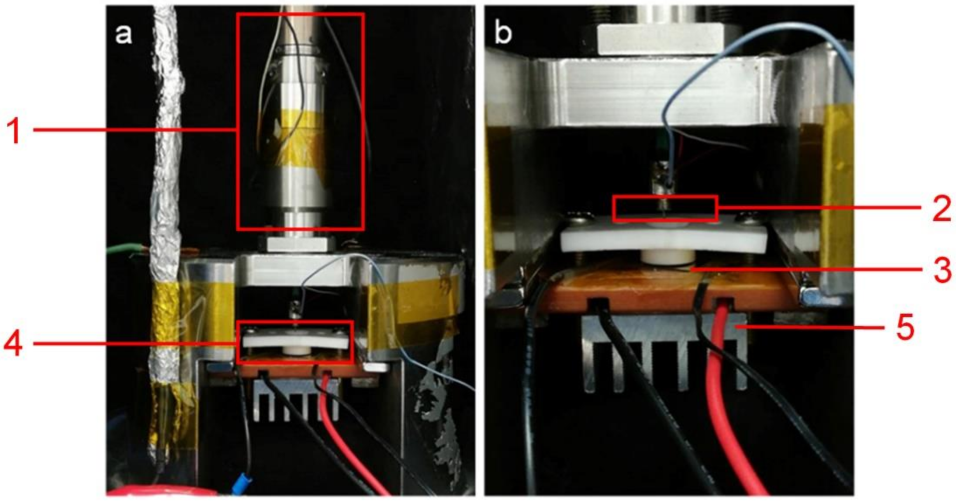

Figure S4. Photo of (a) STM-BJ setup, (b) zoom-in image of STM-BJ setup. 1 denotes the motor, 2 the STM tip, 3 the Au electrode, 4 the teflon liquid cell and teflon O-ring and 5 the Peltier heater.

4. Blank experiment results for pure solvent

We used the pure solvent (THF: TMB, 1: 4) without target molecules as a blank experiment for the calibration of stretching rate of gold tips for break junction experiments. The 1D and 2D conductance histograms show direct tunneling and clear non-plateau features (Fig. S5), suggesting a pure and clean environment inside the cell between tip and substrate. According to the previous measured tunneling decay constant ($\log[\Delta G/G_0]/\Delta z$ = -5.5 nm^{-1}) in the same solvent using break junction technique,[1] we calibrate the relative displacement (Δz) in the conductance ranging from $10^{-0.5}$ to $10^{-6.0}$ G_0 to be ~0.50 nm, as shown in inset of Fig. S5b.

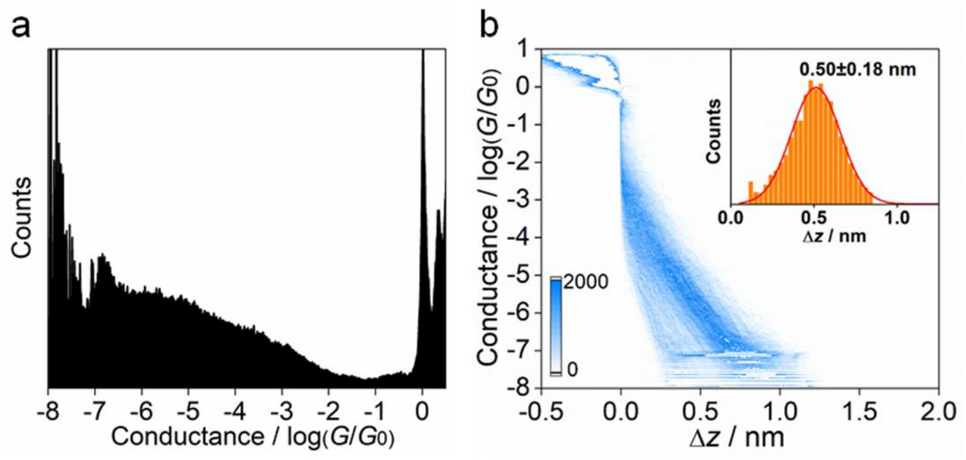

Figure S5. (a) 1D conductance histogram, (b) 2D conductance histogram and versus relative distance (Δz) of the pure solvent. The relative displacement distributions were determined from $10^{-0.5}$ to $10^{-6.0}$ G_0. The clean background also suggests the noise floor is below 10^{-7} G_0. The relative displacement (~0.50 nm) for pure solvent with non-plateau features is ascribed to the snap-back effect of gold-gold contact.

5. Formation probabilities of single-molecule junctions

To determine the junction formation probability[3] of single-molecule junctions quantitatively, we analyzed the formation probability of single-molecule junctions for MHOH and the carbocation by spectral clustering algorithm[4]. In general, conductance traces with plateaus are intrinsically composed of both through-space tunneling (background tunneling) and through-molecule tunneling contributions. Therefore we divided the original single-molecule conductance data (Cluster 0) into two categories: one is background tunneling (Cluster 1) and the other is molecular tunneling (Cluster 2). The formation probability of single-molecule junctions can be determined by the ratio of the traces with molecular tunneling in all traces. The results show that the junction formation probabilities are between 40% and 50% for the both molecular junctions. Compared with the molecular system with weak interactions binding to gold[5], the carbocation-based molecular junctions form with relatively high probabilities.

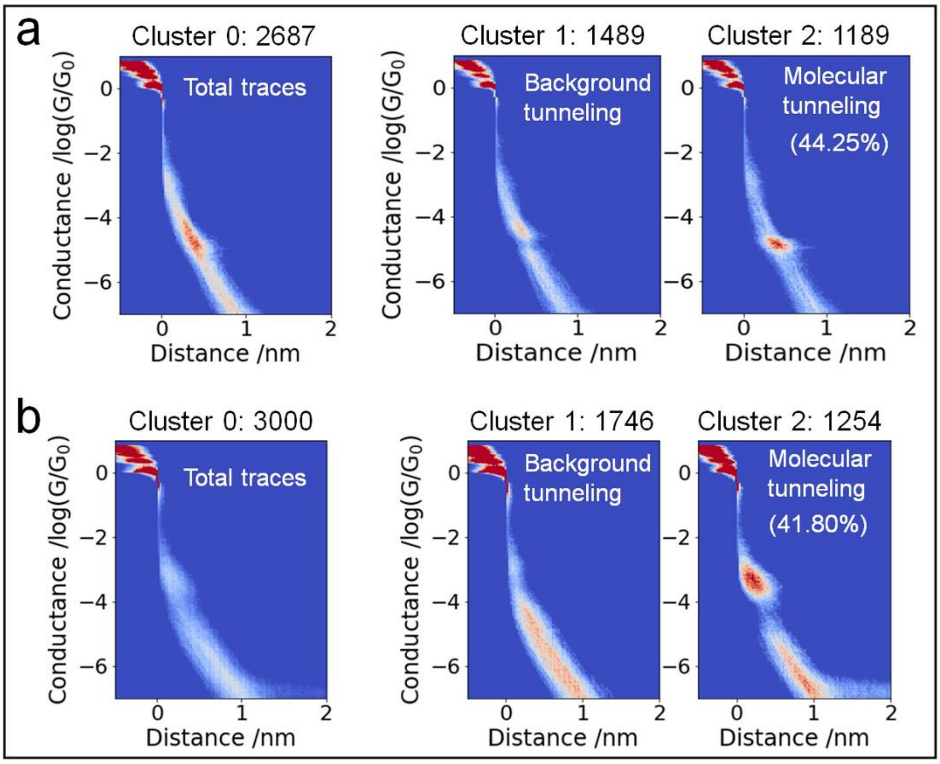

Figure S6. Quantitative analysis of the formation probability of molecular junctions for MGOH and the carbocation. 2D conductance-distance histograms for MGOH (a) and the carbocation (b). The Data in Cluster 0, Cluster 1 and Cluster 2 represent total traces, background tunneling and molecular tunneling, respectively. A number of conductance versus distance traces (typically 2000-3000 traces) were obtained for statistical analysis. For the data analysis, we processed all data without any selection and normalization.

The spectral clustering algorithm is a state of art clustering technique which provides a partition of data and assigns similar data traces into clusters. Here we firstly review the spectral clustering algorithm according to the *Ng et al*.[4] on the 1D conductance histograms.

Given histogram data $H = \{h_1, h_2, ..., h_M\}$ in $\boldsymbol{R}^N$ (dividing the conductance axis to discrete N bins) that we want to cluster into K clusters:

1. Form the affinity matrix $\boldsymbol{A} \in \boldsymbol{R}^{M\times M}$ defined by $\boldsymbol{A}_{ij} = \boldsymbol{C}_{ij} + 1$ if $i \neq j$, and $\boldsymbol{A}_{ii} = 0$.
2. Define $\boldsymbol{D}$ to be the diagonal matrix whose (i, j)-element is the sum of $\mathbf{A}$'s i-th row, and construct the matrix $\boldsymbol{L}=\boldsymbol{D}^{-1/2}\boldsymbol{A}\boldsymbol{D}^{-1/2} - \boldsymbol{I}$.

3. Find x_1, x_2, ... x_K, the K largest eigenvectors of $\boldsymbol{L}$, and form the matrix $\boldsymbol{X} = [x_1, x_2, \ldots x_K]$ belong to $\boldsymbol{R}^{M \times K}$ by stacking the eigenvectors in columns.
4. Treating each row of $\boldsymbol{X}$ as a point in $\boldsymbol{R}^K$, cluster them into K clusters via K-means++.
5. Finally, assign the original points h_i to cluster j if and only if row i of the matrix $\boldsymbol{X}$ was assigned to cluster j.

Here we construct the affinity matrix A specified different from the usual one (the Gaussian (aka RBF) kernel), the other steps are almost the same as described in *Ng et al.*[2] Here we define the $\boldsymbol{C}_{ij}$ as the cross-correlation between histogram h_i and h_j as follow:

$$\boldsymbol{C}_{ij} = \frac{\langle [h_i - \langle h_i \rangle][[h_j - \langle h_j \rangle] \rangle}{\sqrt{\langle [h_i - \langle h_i \rangle]^2 \rangle \langle [h_j - \langle h_j \rangle]^2 \rangle}} \tag{1}$$

where $\langle h_i \rangle$ represents the average value of histogram h_i, the values of $\boldsymbol{C}$ range from [-1, 1], so we add one to make the elements of affinity matrix $\boldsymbol{A}$ nonnegative to meet the spectral clustering requirements. h_i is the conductance histogram for the i-th individual trace, M is the number of conductance traces, N is the number of the histogram bins.

6. Control experiments

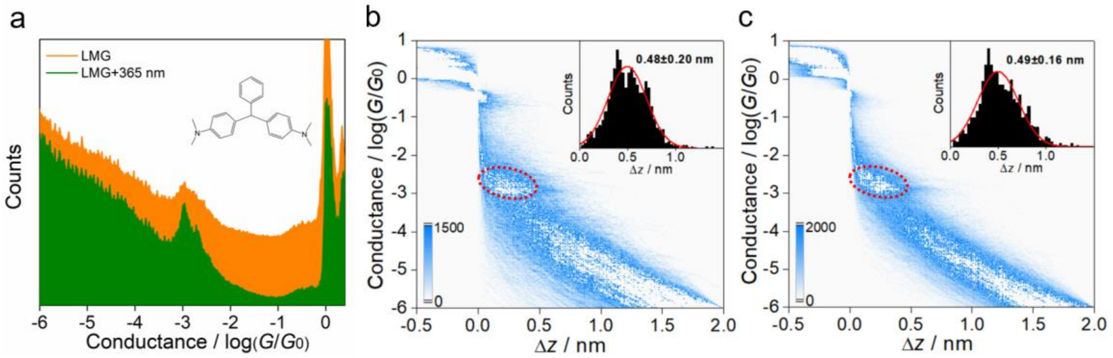

Figure S7. (a) 1D conductance histograms of 4,4'-bis(dimethylamino)triphenylmethane leucohydroxide (LMG) without illumination (orange) and with the *in-situ* illumination (green). The inset shows the molecular structures of LMG. 2D conductance histograms of LMG without illumination (b) and with the *in-situ* illumination (c). The plateau relative displacement distributions for both molecular junctions are shown in the inset of (b) and (c). For there is no obvious conductance change observed, the light with 302 nm seems to have little influence on the molecular conductance of LMG. We noted that LMG has a higher conductance even than the carbocation. In order to account for this phenomenon, we carried out UV-Vis spectrum for LMG as shown in Fig. S8 and the results show that LMG exhibits single peak at 306 nm, which is similar with that of MGOH. Actually, in some ways, the electrical properties of single molecules are highly complicated, which associates not only with the molecular structure such as substituent groups, but also with molecular conformations[6] and other factors. So, it is necessary to combine theoretical calculations including molecular dynamics simulations[7] and experimental observations to get a reasonable explanation for the electrical properties of single molecules. We have not yet completely studied the single-molecule electrical properties for LMG by further theoretical research and experiment, but we think it is a very interesting thing to study the higher conductance of LMG compared to that of MGOH. The rigorous and fully theoretical explorations on the high-conductance for LMG is on the way in our lab.

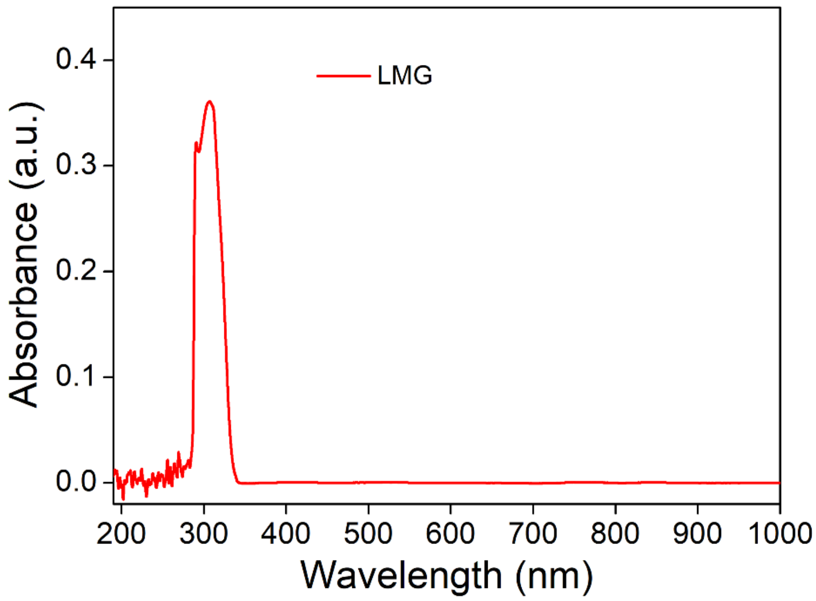

Figure S8. UV-Vis spectrum of LMG in the mixed solvent (THF: TMB, 1: 4).

7. Stability experiments in different solvents

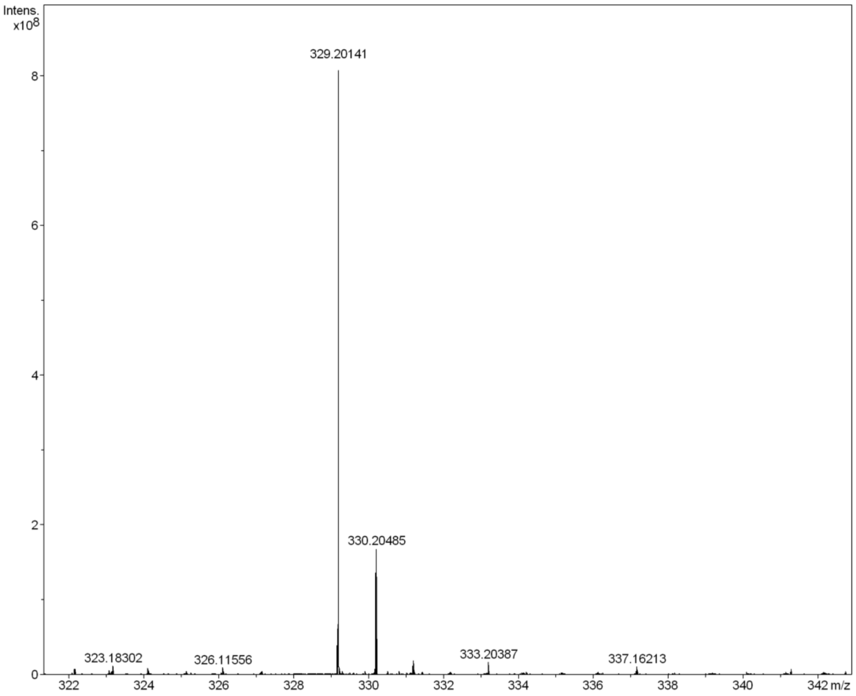

Figure S9. ESI-MS spectra of carbocations after illumination with MGOH for 7 days. Calculated M(MG^+) = 329.20, ESI, found: m/z 329.20141: $[M]^+$; 330.20485: $[M + H]^+$.

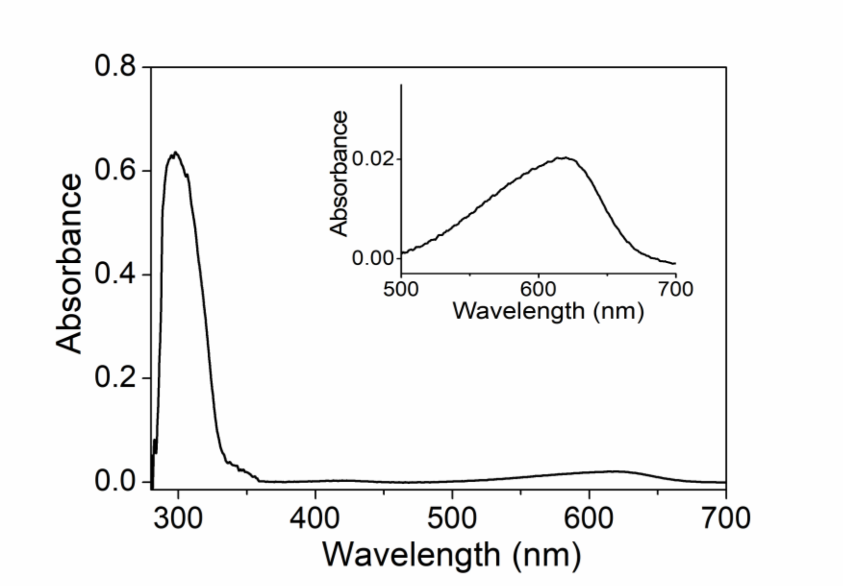

Figure S10. UV-Vis spectrum of the carbocation after illumination with MGOH for 7 days. Although the peak at ~610 nm is much lower than that of the carbocation after forming within 3 min, but this characteristic peak for the carbocation are still clear.

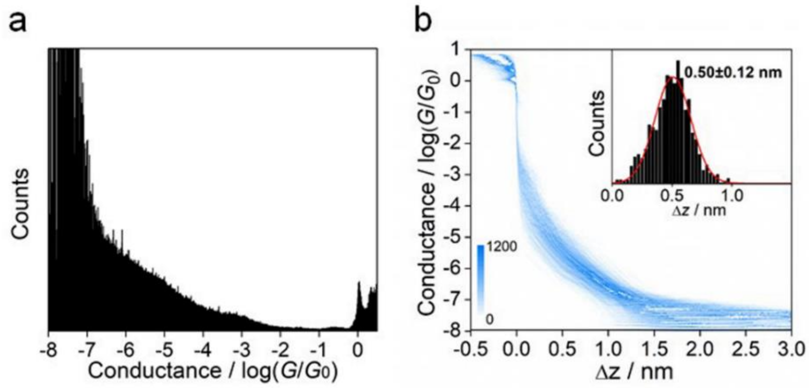

Figure 11. (a) 1D conductance histogram and (b) 2D conductance of the mix solution including four molecules (4-(dimethylamino)phenol, (4-(dimethylamino)phenyl)(phenyl)methanone, 4-hydroxybenzoic acid and benzene). The concentration of each molecule is kept at 0.1 mM. The four molecules are main degradation products of malachite green (Journal of Hazardous Materials, 2013, 260, 585-592 and Chemical Engineering and Processing, 2012, 62, 47-53). The inset shows characteristic length distribution from $10^{-0.5}$ to $10^{-6.0}$ G_0 in the experiment. For the degradation, the malachite green is converted into products including 4-(dimethylamino)phenol and these degradation products aren't form a molecular junction for conductance measurement.

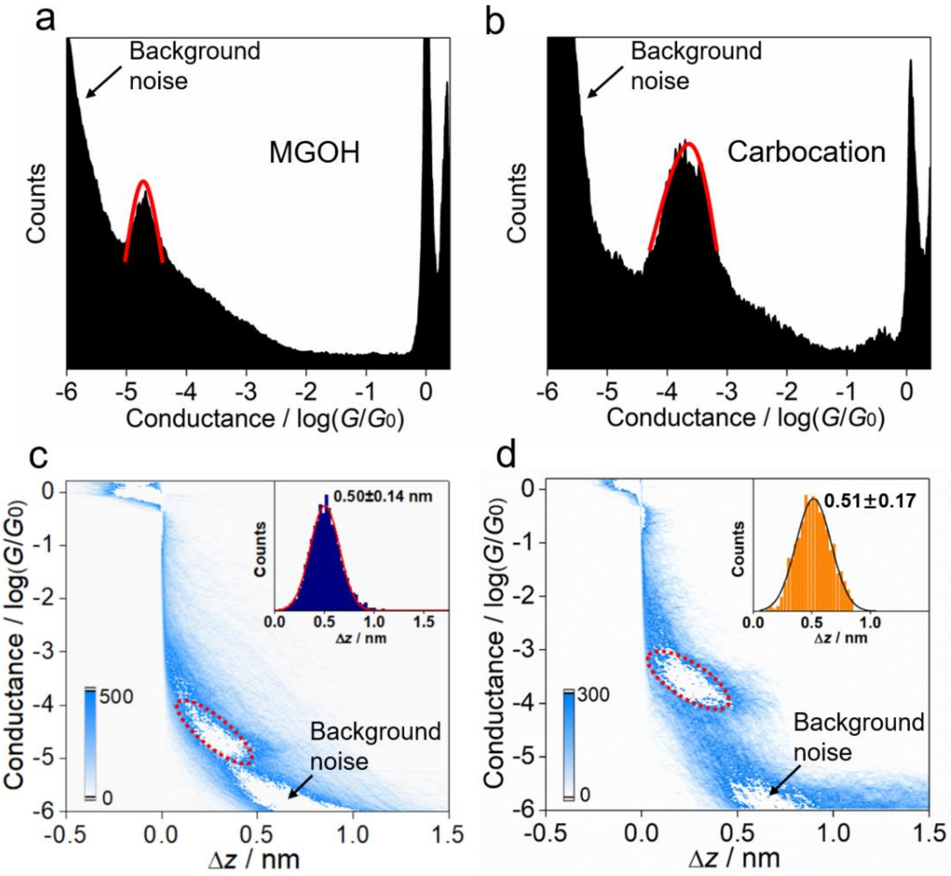

Figure 12. Single-molecule conductance of MGOH and the carbocation when measured after 7 days. (a and b) 1D conductance histogram of MGOH and the carbocation, (c and d) 2D conductance histogram and versus relative distance (Δz) of MGOH and the carbocation. The relative displacement distributions were determined from $10^{-0.5}$ to $10^{-6.0}$ G_0.

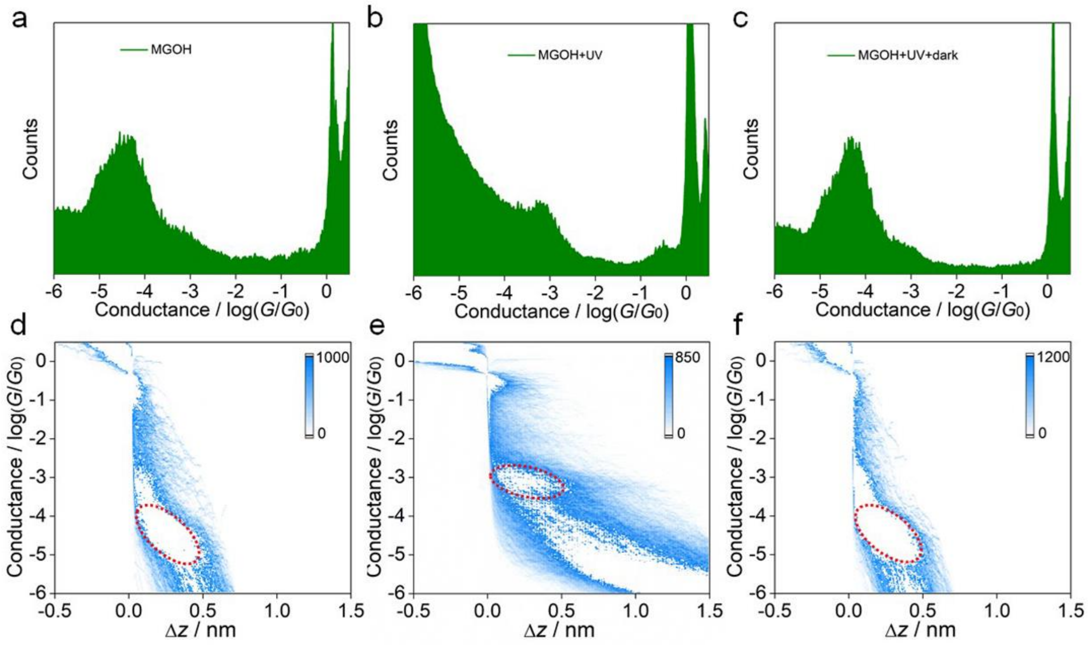

Figure S13. Conductance measurements in aqueous solution. 1D conductance histograms for MGOH in aqueous solution without illumination (a), with the *in-situ* illumination (b). (c) Measured 1D conductance results of the carbocation-based junctions after 90 mins in the dark. (d, e, f) represent the corresponding 2D conductance histograms for a, b, c, respectively.

8. DFT calculations

We first calculated the Au-N binding energies in both molecular junctions. All the density functional theory (DFT) calculations were performed using the Gaussian 16 program package with the tight SCF convergence criterion and fine integration grids. The geometry optimization of Au cluster was accomplished at the B3LYP/SDD level. The basis set of MGOH and carbocation were B3LYP/6-311*. This basis set was enough for single point energy calculation. This basis set was enough for single point energy calculation. Hybrid basis set was used for binding energy calculations of Au-MGOH and Au-carbocation. In the process of geometry optimization of the molecules, the energy tends to the minimum gradually. The energy values of gold clusters and molecules are constant, and the calculation formula of binding energy is as follows:

$$E_{binding} = E_{Au\text{-}molecule} - (E_{Au} + E_{molecule})$$

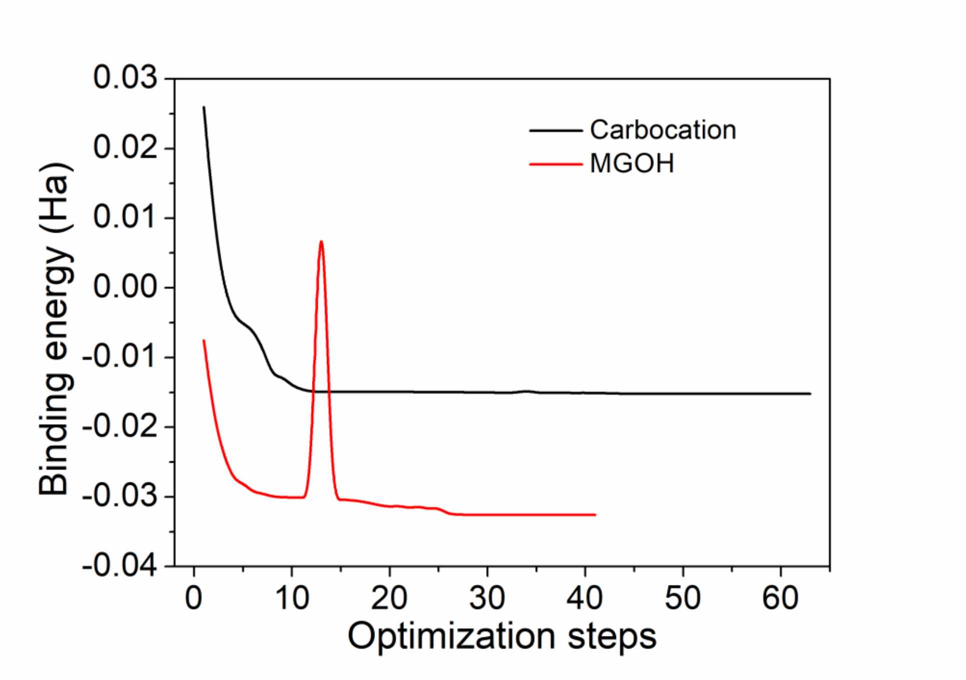

Figure S14. Calculation of the binding energies for MGOH and the carbocation.

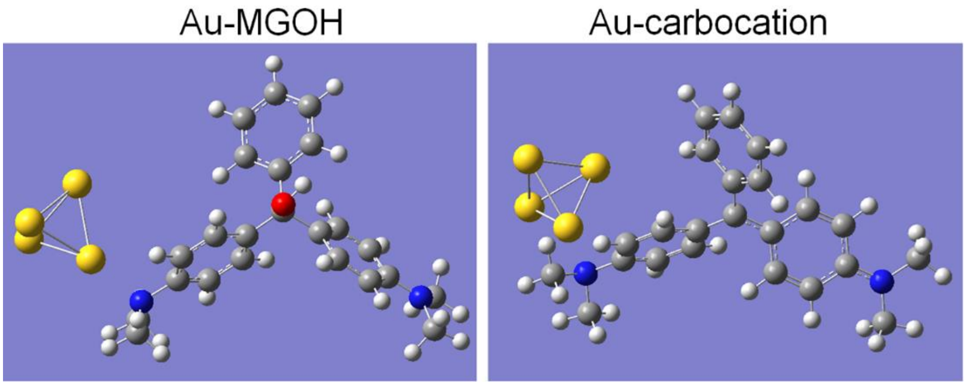

Figure S15. Optimized geometries for MGOH and the carbocation.

Next, we calculated their transmission spectra using the non-equilibrium Greens function (NEGF) formalism with DFT. All structures for frontier molecular orbitals visual output were optimized at B3LYP /6-311G (d, p) level of DFT.[8-11] All the optimizations were performed with the Gaussian 16 software package[12] at 298 K. In addition, the frequency calculations were performed to confirm the characteristics of the calculated structures as minimal.

The transmission spectra were obtained by using density functional theory (DFT) combined with the non-equilibrium Green's function (NEGF) method as implemented in the QuantumATK 2018.6 software package.[13-15] To construct such single-molecule device models, all the molecules were optimized by Gaussian 16 as described above. Then, each target molecule was attached to the gold atoms at two gold electrodes to fabricate the typical gold-molecule-gold model. The initial Au-N distance is 2.7 Å. The geometry of the entire scattering region is relaxed until all residual forces on each atom are less than 0.05 eV/Å. The GGA-PBE exchange-correlation functional was adopted. SZP basis set is for Au atoms and DZP basis set is for the other atoms.

For coherent tunneling, the conductance through a molecular junction at room temperature in the zero-bias limit can be given by the Landauer formula[16]

$$\mathrm{G}(E_F) = \frac{2e^2}{h} \int T(E) \left(-\frac{df}{dE}\right) dE$$

where $T(E)$ is the transmission function, f is the Fermi distribution. For the complexed molecules an average is taken over all calculated geometries.

For electrons of energy E passing through a single molecular orbital, the simplest description of Breit-Wigner resonances is provided by the Breit-Wigner formula[17-19]

$$\mathrm{T(E)} = 4\Gamma_1\Gamma_2/[(E-\varepsilon_n)^2 + (\Gamma_1+\Gamma_2)^2]$$

where T(E) is the transmission function, Γ_1 and Γ_2 describe the coupling of the molecular orbital to the electrodes (labeled Γ_1 and Γ_2) and n = En - Σ is the eigenenergy En of the molecular orbital shifted slightly by an amount Σ due to the coupling of the orbital to the electrodes.

The formula is valid when the energy E of the electron is close to an eigenenergy Ɛn of the isolated molecule, and if the level spacing of the isolated molecule is larger than ($\Gamma_1 + \Gamma_2$). This formula shows that when the electron resonates with the molecular orbital (i.e. when E = Ɛn), electron transmission is a maximum. In the case of carbocation-based junctions, the symmetric molecule attached symmetrically to identical leads, $\Gamma_1 = \Gamma_2$ and therefore, when E = Ɛn, the on-resonance value of T(E) = 1. Thus, the resonance condition (E = Ɛn) described by the Breit-Wigner formula makes carbocation-based junctions display high-conductance characteristics.

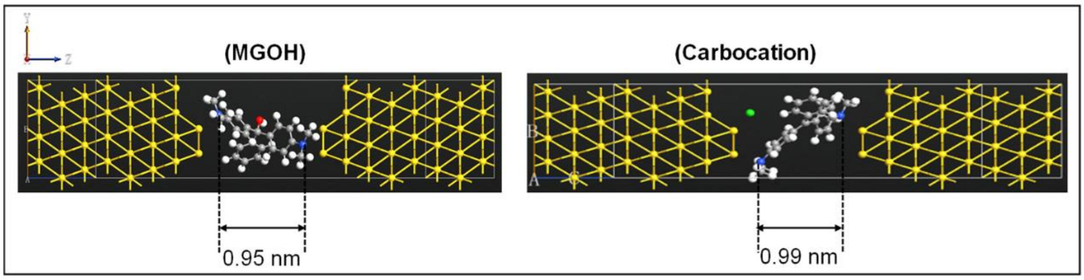

Figure S16. Molecular configurations of MGOH (left) and carbocations (right) in gold electrodes. It should be noted that NEGF-DFT based formalism can't straight-forward to calculate transmission of a charged molecule as the gold electrodes are electron reservoirs. Therefore we referred to the previous papers[20,21] and added the chlorine ion (counter-ion) to balance the charge of carbocations to calculate its transmission spectra. The green sphere on the right pane represents the chlorine ion. The theoretical molecular length of MGOH and the carbocation are 0.95 nm and 0.99 nm, respectively. Dimethylamino moieties are not commonly used in molecular electronics. Nevertheless, the ability of dimethylamino moieties to anchor to gold has been reported widely in the field of surface-enhanced Raman spectroscopy.[22,23]

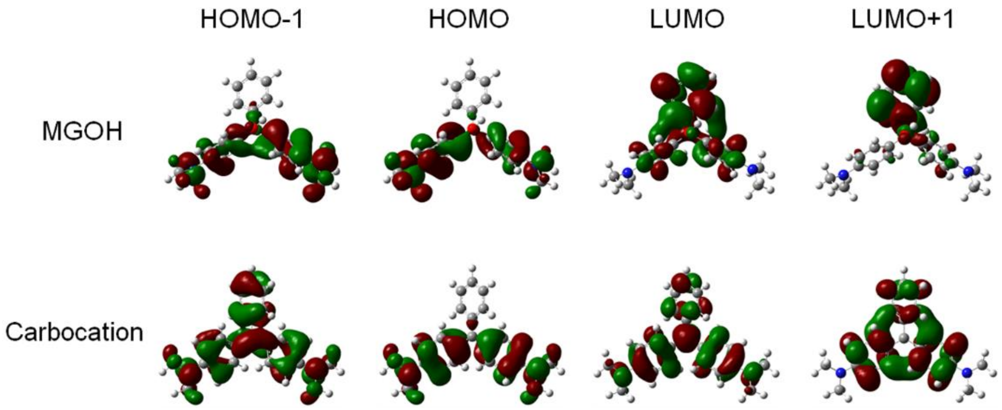

Figure S17. Frontier molecular orbitals (HOMO-1, HOMO, LUMO, LUMO+1) for molecules MGOH and carbocations.

Table S1. Calculated energy levels of frontier molecular orbital of MGOH and carbocations.

Name	HOMO (eV)	LUMO (eV)	Gap (eV)
MGOH	-5.032807	-0.379239	4.653568
Carbocations	-8.385549	-5.795703	2.589847

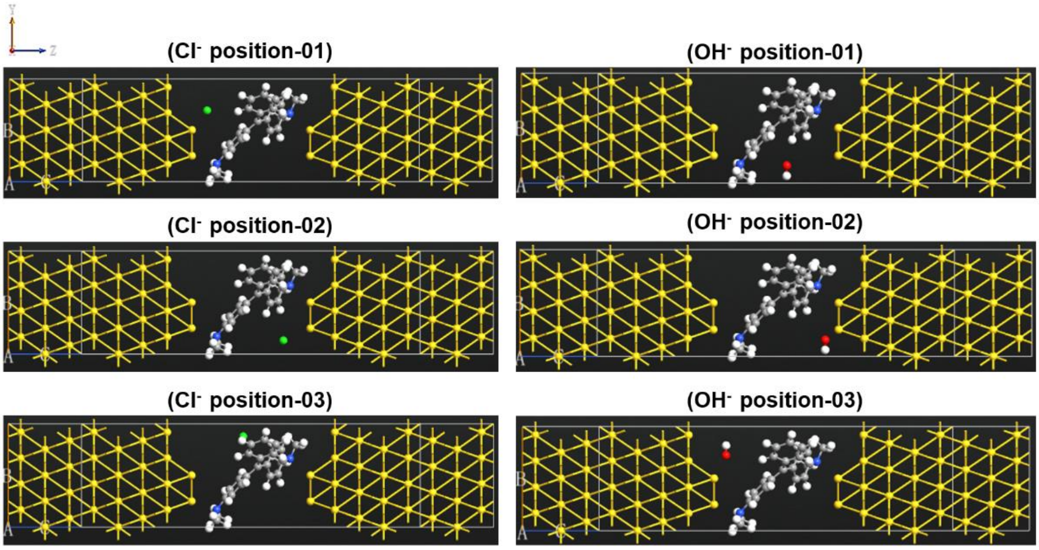

(Cl$^-$ position-01)

(OH$^-$ position-01)

(Cl$^-$ position-02)

(OH$^-$ position-02)

(Cl$^-$ position-03)

(OH$^-$ position-03)

Figure S18. Molecular configurations of carbocations in gold electrodes with different counter-ions in different positions. The green sphere on the left pane represents the chlorine ion; the red-white sphere on the right pane represents the hydroxide ion. These ions are randomly placed.

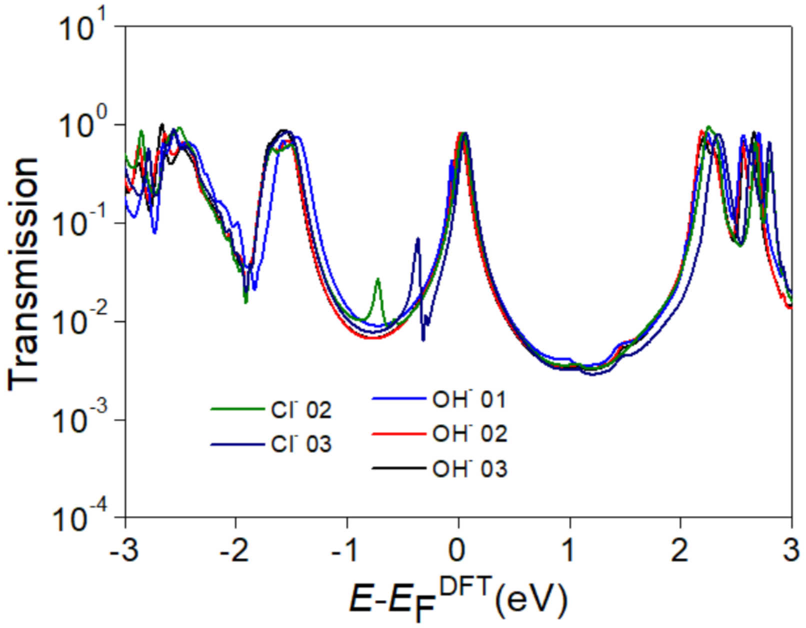

Figure S19. Transmission as a function of energy for the carbocation with different counter-ions in different positions. The transmission spectra for Cl$^-$ at position-01 has been shown in Figure 4 in Page 4 in the manuscript.

9. References

(1) W. Hong, H. Valkenier, G. Meszaros, D. Z. Manrique, A. Mishchenko, A. Putz, P. M. Garcia, C. J. Lambert, J. C. Hummelen and T. Wandlowski, *Beilstein J. Nanotechnol.*, 2011, **2**, 699.

(2) J. Liu, X. Zhao, J. Zheng, X. Huang, Y. Tang, F. Wang, R. Li, J. Pi, C. Huang, L. Wang, Y. Yang, J. Shi, B. Mao, Z. Tian, M. R. Bryce and W. Hong, *Chem*, 2019, **5**, 390.

(3) C. Zhan, G. Wang, X. Zhang, Z. Li, J. Wei, Y. Si, Y. Yang, W. Hong, Z. Tian, *Angew. Chem. Int. Ed.*, 2019, **131**, 14676.

(4) A. Y. Ng, M. I. Jordan and Y. Weiss, *Advances in Neural Information Processing Systems 14*, Vols 1 and 2 2002, **14**, 849.

(5) C. A. Martin, D. Ding, J. K. Sørensen, T. Bjørnholm, J. M. van Ruitenbeek, and H. S. J. van der Zant, *J. Am. Chem. Soc.*, 2008, **130**, 13198.

(6) E. J. Dell, B. Capozzi, K. H. DuBay, T. C. Berkelbach, J. R. Moreno, D. R. Reichman, L. Venkataraman, and L. M. Campos, *J. Am. Chem. Soc.*, 2013, **135**, 11724.

(7) M. Paulsson, *Nano Lett.,* 2009, **9**, 117.

(8) A. D. Becke, *J. Chem. Phys.*, 1993, **98**, 5648.

(9) P. J. Hay and W. R. Wadt, *J. Chem. Phys.*, 1985, **82**, 299.

(10) C. Lee, W. Yang and R. G. Parr, *Phys. Rev. B*, 1988, **37**, 785.

(11) B. Miehlich, A. Savin, H. Stoll and H. Preuss, *Chem. Phys. Lett.*, 1989, **157**, 200.

(12) M. Frisch, G. Trucks, H. Schlegel, G. Scuseria, M. Robb, J. Cheeseman, G. Scalmani, V. Barone, G. Petersson and H. J. I. Nakatsuji, Wallingford CT, 2016.

(13) M. Brandbyge, J.-L. Mozos, P. Ordejón, J. Taylor and K. Stokbro, *Phys. Rev. B*, 2002, **65**.

(14) B. Capozzi, J. Xia, O. Adak, E. J. Dell, Z. F. Liu, J. C. Taylor, J. B. Neaton, L. M. Campos and L. Venkataraman, *Nat. Nanotechnol.*, 2015, **10**, 522.

(15) Z.-Q. Fan and K.-Q. Chen, *Appl. Phys. Lett.*, 2010, **96**.

(16) L. Sun, Y. A. Diaz-Fernandez, T. A. Gschneidtner, F. Westerlund, S. Lara-Avila and K. Moth-Poulsen, *Chem. Soc. Rev.*, 2014, **43**, 7378.

(17) I. A. Shelykh and N. G. Galkin, *Phys. Rev. B*, 2004, **70**.

(18) A. Vezzoli, I. Grace, C. Brooke, K. Wang, C. J. Lambert, B. Xu, R. J. Nichols and S. J. Higgins, *Nanoscale*, 2015, **7**, 18949.

(19) K. Wang, A. Vezzoli, I. M. Grace, M. McLaughlin, R. J. Nichols, B. Xu, C. J. Lambert and S. J. Higgins, *Chem. Sci.*, 2019, **10**, 2396.

(20) Z. Li, M. Smeu, S. Afsari, Y. Xing, M. A. Ratner and E. Borguet, *Angew. Chem. Int. Ed.*, 2014, **53**, 1098.

(21) J. Liu, X. Zhao, Q. Al-Galiby, X. Huang, J. Zheng, R. Li, C. Huang, Y. Yang, J. Shi, D. Z. Manrique, C. J. Lambert, M. R. Bryce and W. Hong, *Angew. Chem. Int. Ed.*, 2017, **56**, 13061.

(22) S. Lee, H. Chon, M. Lee, J. Choo, S. Y. Shin, Y. H. Lee, I. J. Rhyu, S. W. Son, C. H. Oh, *Biosens. Bioelectron.*, 2009, **24**, 2260.

(23) J. Gong, J. Jiang, H. Yang, G. Shen, R. Yu, Y. Ozaki, *Anal. Chim. Acta*, 2006, **564**, 151.